

Longitudinal and transverse mode coupling instability: Vlasov solvers and tracking codes

E. Métral 

CERN, 1211 Geneva, Switzerland

M. Migliorati *

University of Rome La Sapienza and INFN, Sez. Roma1, 00185 Rome, Italy



(Received 1 May 2020; accepted 23 June 2020; published 6 July 2020)

The study of collective effects in circular accelerators can be tackled by solving numerically the Vlasov equation or by using tracking codes. The two methods are obtained with different approaches: Vlasov solvers consider a continuous distribution function and describe the beam with coherent oscillation modes in frequency domain (ending up usually with an eigenvalue system to solve), while tracking codes use macroparticles and wakefields in time domain. In this paper we present two Vlasov solvers for the study of collective effects (from impedances/wakefields only) which evaluate the frequency shift of coherent oscillation modes and possible mode coupling instability in the single-bunch case for both longitudinal and transverse planes. In the longitudinal plane the Vlasov solver also takes into account the potential well distortion due to the wakefields under some conditions. In parallel to this theoretical approach, tracking codes, which include collective effects, have been used as benchmark. In particular, starting from their results, we also propose a new method to study the frequency shift of coherent modes and compare it with the output of the Vlasov solvers.

DOI: [10.1103/PhysRevAccelBeams.23.071001](https://doi.org/10.1103/PhysRevAccelBeams.23.071001)

I. INTRODUCTION

Collective effects in circular accelerators can be studied by taking into account, in a self-consistent way and in addition to external guiding fields, the effects of self-induced wakefields [1–3]. One important consequence of these fields is the generation of instabilities. Generally, for the study of beam dynamics, it is convenient to distinguish between the longitudinal and transverse planes. This is true for many accelerators [4–6] except when synchrotron resonances become important. Another distinction which helps to simplify the study of collective effects is related to single-bunch or multibunch beam dynamics generated by short or long-range wakefields, respectively.

The theoretical approach to the instabilities due to collective effects, whether they are single or multibunch, considers the beam as a continuous distribution function and expands it as a superposition of coherent oscillation modes perturbed by the wakefields. Actually the analysis is performed in frequency domain with the use of the concept of coupling impedance, which represents the Fourier transform of the wakefield (in fact of the wake function

to be more precise). One limit of this analysis is the fact that we resort to a linear perturbation theory, which fails when nonlinearities, e.g. for Landau damping, become important.

For the study of the beam dynamics in the presence of collective effects, a tracking code represents nowadays a very reliable tool. The bunch is considered as an ensemble of macroparticles (generally around 10^6 – 10^7) and their equations of motion can be easily integrated in time domain by taking into account the wakefields [7–10]. This generally requires the necessity of quite heavy computing resources. Of course the use of discrete macroparticles makes simulation codes complementary to the theoretical approach of modal expansion.

Another ingredient to take into account when dealing with instabilities in circular accelerators is the total machine impedance and the corresponding wakefield. Several devices contribute to it, as, for example, resistive wall [11–14], space charge [15–18], collimators [19,20], and so on. The impedance of an accelerator is generally a very complicated function of frequency with many peaks (due to resonant modes) influencing the multibunch beam dynamics (as this corresponds to long-range wakefields) and a smoother impedance of broadband kind affecting the single-bunch beam dynamics (as this corresponds to short-range wakefields) [21]. Therefore, the machine impedance, in some conditions, can be replaced by some broadband impedance model, which is characterized by a small number of parameters [22–25] simplifying the study of single-bunch instabilities.

*mauro.migliorati@uniroma1.it

Published by the American Physical Society under the terms of the *Creative Commons Attribution 4.0 International license*. Further distribution of this work must maintain attribution to the author(s) and the published article's title, journal citation, and DOI.

In this paper, focusing on protons, we present two Vlasov solvers which allow to obtain the frequencies of coherent oscillation modes describing the beam motion in the single-bunch case for the longitudinal and transverse planes, and compare their results with a novel method which analyzes directly the macroparticle motion obtained as output from tracking simulation codes, and allows determining the analogous coherent frequencies without recurring to Vlasov solvers. Moreover, the same method can also be used with direct beam measurements.

In the next section of this paper we discuss the machine parameters that we have used for the study, and, in Sec. III we describe the two Vlasov solvers, for the longitudinal and transverse planes, comparing them to other Vlasov solvers currently used by the community [26–28]. Then, in Sec. IV we discuss a new method proposed to evaluate the frequencies of coherent oscillation modes starting from the output of macroparticle simulation codes, and, in Sec. V, we compare these results with those of the Vlasov analysis in both planes. In Sec. VI simple analytical formulas for the instability thresholds are provided, which reveal the different mitigation methods, and a final section is dedicated to concluding remarks.

II. BEAM AND MACHINE PARAMETERS

In order to benchmark the results of the two approaches, we used the CERN Super Proton Synchrotron (SPS) machine parameters, but adapted to our specific context. In particular, for the machine we considered the relativistic mass factor $\gamma = 27.73$, the relativistic mass factor at transition $\gamma_{tr} = 22.77$ (with the machine working therefore above transition energy), the circumference $C = 6911$ m, the peak rf voltage $V_{rf} = 6$ MV, and the harmonic number $h = 462$. This last value does not correspond to the actual one used in the SPS (4620) because, for the comparisons, we wanted to be in the linear part of the rf voltage in order to minimize possible effects due to the nonlinearities of the longitudinal phase space. Thus, by reducing the harmonic number, we increased the rf bucket maintaining constant the bunch length, which we chose with a parabolic line density distribution for the longitudinal case with a full length (4σ) equal to $\tau_b = 2.7$ ns at low intensity.

With the above machine parameters, the unperturbed synchrotron tune is $Q_{s0} = 3.26 \times 10^{-3}$. For the transverse beam dynamics, in addition to the above parameters, we considered a smooth lattice with a transverse low-intensity tune of $Q_{x0} = 26.13$.

For what concerns the collective effects, let us consider the *RLC* impedance model that, in the longitudinal plane, can be written as

$$Z_{\parallel}(f) = \frac{R_{\parallel,s}}{1 + jQ\left(\frac{f}{f_r} - \frac{f_r}{f}\right)}. \quad (1)$$

A special case of the *RLC* model is the broadband resonator (BBR) that has typically the quality factor $Q = 1$, and that we have used through all of this paper. For the other parameters, we considered the following values: resonant frequency $f_r = 1$ GHz, such that $f_r\tau_b = 2.7$, and shunt impedance $R_{\parallel,s} = 2 \times 10^5 \Omega$. The chosen bunch length gives a cutoff frequency quite below the BBR resonant frequency so that we have a bunch interacting principally with the imaginary part of the low frequency impedance as shown in Fig. 1 where we have reported the real and absolute imaginary part of the BBR impedance (blue and orange curves) evaluated at $f = pf_0$, with p an integer number and f_0 the revolution frequency, and divided by p together with the bunch power spectrum (green curve in arbitrary units) which is such that [29]

$$|S(f)|^2 \propto \frac{J_{3/2}(f\pi\tau_b)}{(f\pi\tau_b)^{3/2}}, \quad (2)$$

with $J(x)$ the ordinary Bessel function of the first kind.

As can be seen from the figure, the imaginary part of $Z_{\parallel}(p)/p$ is almost constant in all the frequency range of interest. This low frequency imaginary impedance is equal to

$$\left. \frac{Z_{\parallel}(p)}{p} \right|_{p \rightarrow 0} \simeq -j \frac{R_{\parallel,s}f_0}{Qf_r} = -j8.67 \Omega. \quad (3)$$

Since the interaction of the BBR impedance with the bunch is essentially inductive, then the main effect on the longitudinal beam dynamics is an increase of the bunch length (we are above transition) due to the potential well distortion (PWD), but the shape of the bunch remains almost symmetric. There is, however, a small real part of the impedance interacting with the bunch spectrum which does not perturb too much the distribution but which is

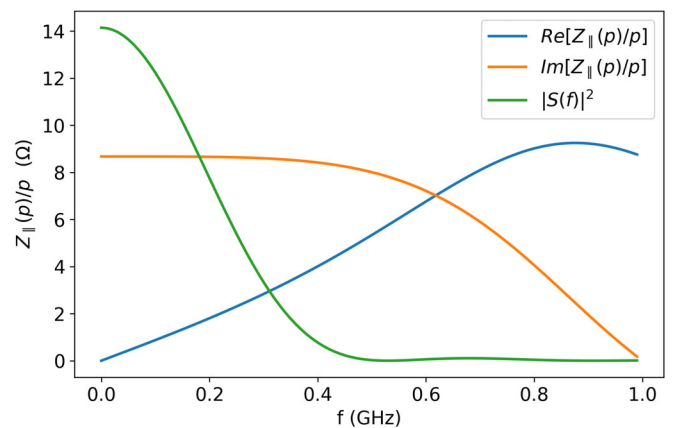


FIG. 1. Real and absolute imaginary part of $Z_{\parallel}(p)/p$ for the BBR impedance as a function of frequency. In the same plot also the bunch spectrum of a parabolic line density distribution with total bunch length of 2.7 ns is represented in arbitrary units.

responsible of the instability as we will see later in the paper.

In addition to the BBR impedance, we have also evaluated the single-bunch longitudinal behavior in the presence of a pure inductive impedance. This corresponds to the case when the resonant frequency of the BBR impedance f_r tends to infinity. It is also important to underline that the wakefield of a pure imaginary impedance is proportional to the derivative of the Dirac delta function, and some simulation codes cannot be run with this kind of impedance.

For the transverse plane we have used a longitudinal bunch shape having a water-bag distribution [29] with the same total bunch length of $\tau_b = 2.7$ ns, and a transverse BBR impedance of the kind

$$Z_{\perp}(f) = \frac{f_r}{f} \frac{R_{\perp,s}}{1 + jQ(\frac{f}{f_r} - \frac{f_r}{f})}, \quad (4)$$

with $R_{\perp,s} = 1$ M Ω /m. The quality factor and the resonant frequency are the same as in the longitudinal case.

III. GALACTIC AND GALACLIC

GALACTIC stands for Garnier-Laclare coherent transverse instabilities code, while GALACLIC stands for Garnier-Laclare coherent longitudinal instabilities code [30]. The approaches used by the two codes are very similar, solving the linearized Vlasov equation as discussed in [29,31]. In Ref. [29], Laclare presented a very nice formalism with a clear procedure to treat both longitudinal and transverse planes, first for the low-intensity case (i.e., when the modes can be treated independently) and then for the general high-intensity case (when the modes cannot be treated independently). One starts with the single-particle motion, which is approximated by the one of a harmonic oscillator with the corresponding beam-induced electromagnetic forces in the longitudinal and transverse planes. Then, one looks at the spectrum of the single-particle signal, which is a line spectrum (around every harmonic of the revolution frequency, there is an infinite number of synchrotron satellites m) centered at 0 for the longitudinal plane and at the chromatic frequency for the transverse plane. A distribution of particles (particle density in phase space) is then considered and expressed as a sum of a stationary distribution and a perturbation. The beam-induced electromagnetic force can be expressed through the impedance, which is a complex function of frequency, for both longitudinal and transverse planes. In this respect, the case of the longitudinal plane is a bit more involved as one has first to study the effect of the impedance on the stationary distribution (i.e., the PWD): a new fixed point is then obtained, with a dependency of the synchronous phase, the incoherent frequency, the effective (total) voltage and the bunch length on the bunch intensity. Around the

new fixed point, one writes the perturbation, which is coherent with respect to the satellite number m . Applying the Vlasov equation to first order, one ends up with an eigenvalue system to solve. The result is an infinite number of modes of oscillation mq (as there are 2 degrees of freedom, the longitudinal amplitude and phase), with m the azimuthal mode number and q the radial one. The latter is defined as $q = |m| + 2k$ (with k an integer between 0 and infinity): with this definition, q represents the number of nodes of the superimposed low-intensity standing-wave patterns, which is a usual observable in particle accelerators. Finally, for the general high-intensity cases (both in longitudinal and transverse), the final eigenvalue systems are obtained by summing over all the modes m . Therefore, the general case is obtained very elegantly by Laclare, leading to eigenvalue systems to solve, but the problem is that the unknown frequency is inside the matrices to be diagonalized. Laclare proposed a procedure to solve them but it seems that only the real part of the mode-frequency shifts can be obtained. The drawbacks of this method are on one hand that it does not allow to follow the individual modes, and on the other hand it does not provide (at least not straightforwardly) the imaginary part of the mode-frequency shifts (which is proportional to the instability growth rate). The latter is very important to check whether the beam is unstable or not. This is why Garnier and Laclare [31] proposed to use a decomposition on the low-intensity eigenvectors to obtain an eigenvalue system with the unknown frequency outside the matrix to be diagonalized. The final result is described by the following two equations [31]:

$$\sigma(l) = \sum_{i,j=-\infty}^{\infty} a_{ij} \sigma_{ij}(l), \quad (5)$$

$$\frac{\omega_c}{\omega_s} a_{kl} = H a_{ij}, \quad (6)$$

where the (general, high-intensity) eigenvector σ is decomposed on the low-intensity eigenvectors σ_{ij} (solutions of the low-intensity eigenvalue problem with pure inductive impedance, which requires two indices as discussed above due to the 2 degrees of freedom, see below), with the coefficients a_{ij} , which can be identified by finding the eigenvectors of the eigenvalue system below, l is an integer, ω_c the (complex) angular frequency (with respect to the angular betatron frequency in transverse), ω_s the angular synchrotron frequency and H is the matrix to be diagonalized. In the case of the transverse plane, the matrix is given by (presenting the results slightly differently compared to Garnier [31])

$$H_{kl,ij}^{\perp} = k \delta_{ki} \delta_{lj} + \Delta \omega_{ckl} \sum_{p=-\infty}^{\infty} \frac{Z_{\perp}(p)}{Z_{\perp}(0)} \sigma_{kl}^*(p) \sigma_{ij}(p), \quad (7)$$

while for the longitudinal plane it is given by

$$H_{kl,ij}^{\parallel} = k\delta_{ki}\delta_{lj} + \Delta\omega_{ckl} \sum_{p=-\infty}^{\infty} \frac{Z_{\parallel}(p)/p}{Z_{\parallel}(p)/p|_{p \rightarrow 0}} \sigma_{kl}^*(p)\sigma_{ij}(p), \quad (8)$$

where δ is the Kronecker delta, and $*$ stands for the complex conjugate. For both longitudinal and transverse cases, the $\Delta\omega_{ckl}$ and the σ_{kl} are the low-intensity eigenvalues and eigenvectors of the following low-intensity eigenvalue problem to be solved, with pure inductive impedance and for the azimuthal mode m (as discussed above, because of the 2 degrees of freedom, the solutions need to be written with two indexes, which above were called k and l), given by

$$\Delta\omega_{cm}\sigma_m(l) = \sum_{p=-\infty}^{\infty} K_{lp}^m \sigma_m(p), \quad (9)$$

with, for the transverse plane,

$$K_{lp}^m = \frac{jeI_b Z_{\perp}(p)}{2\gamma m_0 c Q_{x0}} \int_{\hat{\tau}=0}^{\infty} J_m(l, \hat{\tau}) J_m(p, \hat{\tau}) g_0(\hat{\tau}) \hat{\tau} d\hat{\tau}, \quad (10)$$

and, for the longitudinal plane,

$$K_{lp}^m = -\frac{2\pi I_b m \omega_s}{\Omega_0^2 \hat{V}_T h \cos \phi_s} \frac{jZ_{\parallel}(p)}{p} \times \int_{\hat{\tau}=0}^{\infty} J_m(l\Omega_0 \hat{\tau}) J_m(p\Omega_0 \hat{\tau}) \frac{dg_0}{d\hat{\tau}} d\hat{\tau}, \quad (11)$$

with

$$J_m(p, \hat{\tau}) = J_m\{(p + Q_{x0})\Omega_0 - \omega_{\xi}\hat{\tau}\}, \quad (12)$$

$$\omega_{\xi} = Q_{x0}\Omega_0 \frac{\xi}{\eta}, \quad (13)$$

where j is the imaginary unit (not to be confused with the index j also used in the matrix coefficient), e the absolute value of the elementary charge, $I_b = N_b e f_0$ the bunch current (with N_b the number of charges and $f_0 = \Omega_0/2\pi$ the revolution frequency), m_0 the particle rest mass, c the speed of light, J_m the Bessel function of m th order, g_0 the distribution function of the longitudinal synchrotron amplitudes $\hat{\tau}$, ξ the (relative) chromaticity, η the slippage factor, \hat{V}_T the total voltage (sum of the rf and the wakefield induced voltage), and ϕ_s the rf phase of the synchronous particle ($\cos \phi_s < 0$ above transition).

The eigenvalues of the H -matrices describe the mode-frequency shifts while the eigenvectors can be used to describe the intrabunch motion [32]. In the case of a BBR impedance, the results can be written in terms of a normalized parameter x which is given by

$$x = \frac{4I_b}{\pi^2 B^3 \hat{V}_T h \cos \phi_s} \frac{\text{Im}[Z_{\parallel}(p)]}{p} \Big|_{p \rightarrow 0}, \quad (14)$$

for the longitudinal plane, while for the transverse one

$$x = \frac{\text{Im}[Z_{\perp}(0)] e I_b}{4\pi\gamma m_0 c Q_{x0} B \omega_s}, \quad (15)$$

with $B = f_0 \tau_b$ the bunching factor. It is important to stress that B , \hat{V}_T and ϕ_s depend on the bunch intensity due to the PWD.

It is worth mentioning that in GALACTIC the effect of a transverse damper (which is not discussed in the present paper) was also added [33], as it was already the case with two other transverse Vlasov solvers widely used by the community, NHTVS [27] and DELPHI [28]. These three Vlasov solvers are similar (with some pros and cons) as concerns the subject of this paper as they are solving the same equation but using different formalisms, and it was checked in the past that on few benchmark cases the same results were obtained [33]. It is also worth mentioning that DELPHI uses the same approach as the famous MOSES code which has been used for several decades (since 1988), where the Sacherer integral equation is solved using a decomposition over Laguerre polynomials of the radial functions [26]. Furthermore, the MOSES code had been already successfully benchmarked against the HEADTAIL macroparticle code in [34]. Other approaches to solve the Vlasov equation in the longitudinal plane, valid in particular for electron machines, can be found in [35–37].

Some benchmarks between Laclare's approach [29] and the GALACTIC and GALACLIC Vlasov solvers described above are shown in Figs. 2–4, where in the ordinate axis we have used the tune Q , or the corresponding tune shift ΔQ with respect to Q_{x0} , which represents the coherent frequency divided by the revolution frequency. For the longitudinal plane, both cases without PWD and with PWD are discussed, to clearly reveal the effect of the PWD. For the case without PWD, the eigensystem is solved and the results are plotted using Q_s , i.e. the intensity-dependent synchrotron tune, whereas for the case with PWD, the results are plotted using Q_{s0} , i.e., the low-intensity synchrotron tune (see Fig. 5) using the following expression:

$$\frac{Q}{Q_{s0}} = \frac{Q}{Q_s} F_{\text{PWD}}, \quad (16)$$

where

$$F_{\text{PWD}} = \frac{Q_s}{Q_{s0}} = \frac{1}{\sqrt{1 - \frac{4x}{\pi}}} \quad (17)$$

for the case of a parabolic amplitude density (PAD) longitudinal distribution or

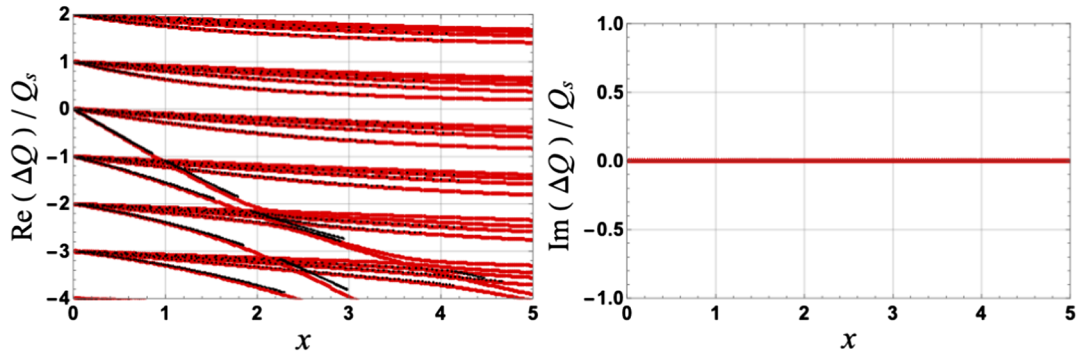


FIG. 2. Comparison between GALACTIC (in red) and Laclare [29] (in black) of the normalized mode-frequency shifts, in the case of a pure inductive impedance and for a water-bag (WB) longitudinal distribution [29]: (left) real part and (right) imaginary part (from GALACTIC only).

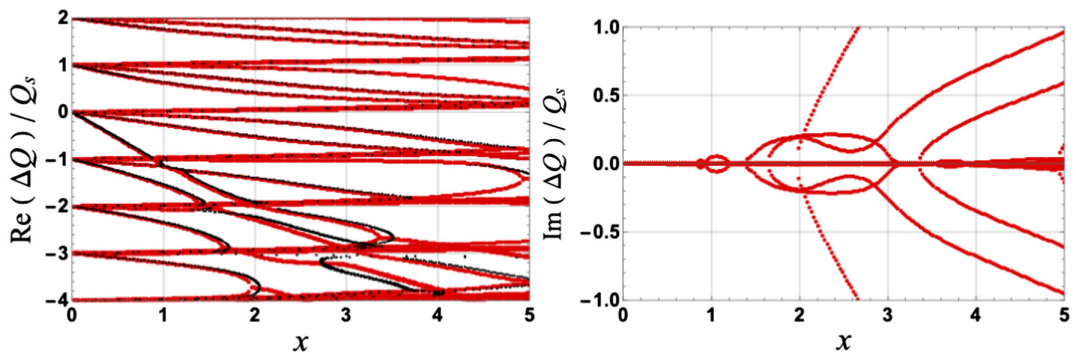


FIG. 3. Comparison between GALACTIC (in red) and Laclare [29] (in black) of the normalized mode-frequency shifts, in the case of a broadband resonator impedance (with a quality factor of 1 and a resonance frequency f_r such that $f_r \tau_b = 2.8$) and for a WB longitudinal distribution [29]: (left) real part and (right) imaginary part (from GALACTIC only).

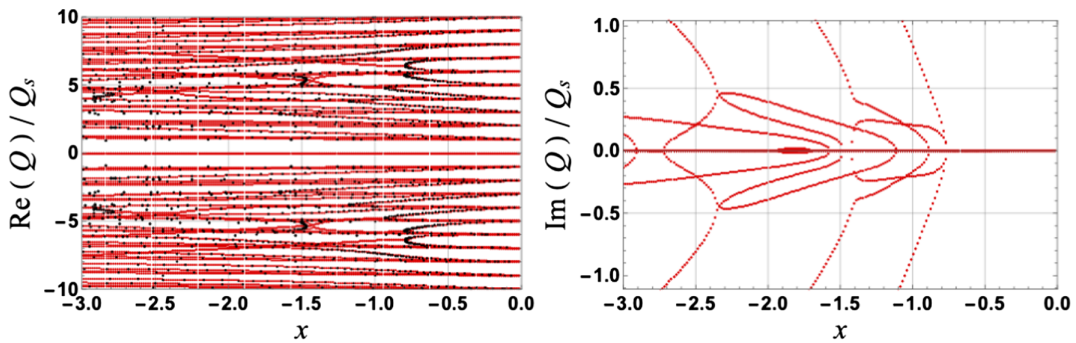


FIG. 4. Comparison between GALACTIC (in red) and Laclare [29] (in black) of the normalized mode-frequency shifts, in the case of a broadband resonator impedance (with a quality factor of 1 and a resonance frequency f_r such that $f_r \tau_b = 2.8$), above transition, without taking into account the PWD and for a parabolic amplitude density (PAD) longitudinal distribution [29]: (left) real part and (right) imaginary part (from GALACTIC only).

$$F_{\text{PWD}} = \frac{Q_s}{Q_{s0}} = \frac{1}{\sqrt{1 - \frac{3x}{4}}} \quad (18)$$

for the case of a parabolic line density longitudinal distribution.

It should be stressed that the case of a bunch in the “long-bunch” regime (where $2f_r \tau_b \gg 1$) is considered here, assuming the simplified case where the shape of the distribution is preserved, i.e. neglecting the effect of the synchronous phase shift. It is worth noticing that the same intensity threshold $x_{th} \approx -0.75$ is obtained for both cases without and with PWD.

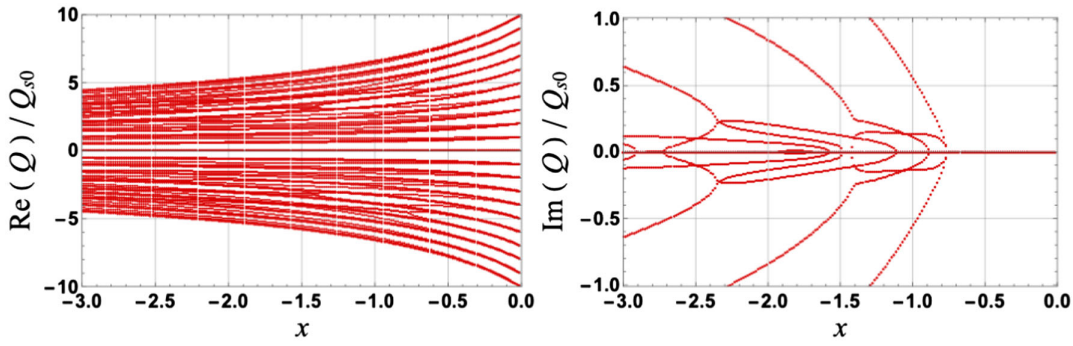


FIG. 5. Normalized (to the low-intensity synchrotron tune) mode-frequency shifts from GALACLIC in the case of a broadband resonator impedance (with a quality factor of 1 and a resonance frequency f_r such that $f_r \tau_b = 2.8$), above transition, taking into account the PWD and for a PAD longitudinal distribution: (left) real part and (right) imaginary part.

IV. TRACKING CODES AND MODAL ANALYSIS

In this section we describe the analysis that can be done starting from the output of a simulation code, which allows one to obtain the frequencies of the coherent oscillation modes to be compared with those of the Vlasov solvers. The method follows closely the theory used to solve the Vlasov equation in both longitudinal and transverse planes.

Let us start with the longitudinal beam dynamics that can be described with the quantities z and ε , which represent the distance and the relative energy variation of a generic particle from the synchronous one. To solve the Vlasov equation by using a linear perturbation technique, as discussed in the previous section, we write the phase space distribution $\Psi(z, \varepsilon; t)$ as a sum of a stationary solution independent on time and a perturbation such that

$$\Psi_{\parallel}(z, \varepsilon; t) = \Psi_{0,\parallel}(z, \varepsilon) + \Psi_{1,\parallel}(z, \varepsilon; t). \quad (19)$$

The perturbation $\Psi_{1,\parallel}(z, \varepsilon; t)$, which is responsible of the instability, is expanded in terms of coherent oscillation modes of the bunch. In order to do that, it is convenient to introduce the pair of longitudinal action-angle coordinates $(J_{\parallel}, \phi_{\parallel})$. Observing that the perturbed distribution function is periodic in ϕ_{\parallel} with a period of 2π , it can be expanded so that

$$\Psi_{1,\parallel}(J_{\parallel}, \phi_{\parallel}; t) = \sum_{m=-\infty}^{\infty} e^{j\Delta\omega_{cm}t} R_{m,\parallel}(J_{\parallel}) e^{-jm\phi_{\parallel}}, \quad (20)$$

with m the index defining the m th azimuthal mode number, $\Delta\omega_{cm}$ its corresponding coherent angular frequency, and $R_{m,\parallel}(J_{\parallel})$ an unknown function of the action variable. In the previous section we have seen how to obtain the coherent angular frequencies in order to determine when the perturbation is unstable (imaginary part of $\Delta\omega_{cm}$ negative) by solving an eigenvalue system. In this section we are not interested to solve numerically the Vlasov equation, but to find a quantity that can be evaluated from the results of a

simulation code giving information on possible coherent oscillation modes. In order to do that, we first observe that the longitudinal distribution function $\lambda(z; t)$ is the projection on the z axis of the phase space distribution $\Psi_{\parallel}(z, \varepsilon; t)$, so that we can also expand this quantity into a stationary solution, determined by the PWD, and a perturbation of the kind

$$\lambda(z; t) = \lambda_0(z) + \lambda_1(z; t), \quad (21)$$

where $\lambda_0(z)$ is normalized to 1, and, from Eq. (20), we can write

$$\begin{aligned} \lambda_1(z; t) &= \int_{-\infty}^{\infty} \Psi_{1,\parallel}(J_{\parallel}, \phi_{\parallel}; t) d\varepsilon \\ &= \sum_{m=-\infty}^{\infty} e^{j\Delta\omega_{cm}t} \int_{-\infty}^{\infty} R_{m,\parallel}(J_{\parallel}) e^{-jm\phi_{\parallel}} d\varepsilon. \end{aligned} \quad (22)$$

Let us now consider the following integral:

$$\begin{aligned} M_{n,\parallel} &= \int_{-\infty}^{\infty} z^n \lambda(z; t) dz \\ &= \int_{-\infty}^{\infty} z^n \lambda_0(z) dz + \int_{-\infty}^{\infty} z^n \lambda_1(z; t) dz. \end{aligned} \quad (23)$$

For $n = 0$ this integral is equal to 1, while, for $n > 1$, it coincides with the n th moment of the distribution in case of symmetric stable bunch, such as the one given by a pure imaginary impedance in the PWD regime. The integral of Eq. (23) can be easily obtained from the results of any simulation code at each integration step (or each turn). Moreover we also observe that, in a real machine, if we are able to measure, turn by turn, the longitudinal distribution function, for example with a tomoscope as done at the CERN proton synchrotron [38], a postprocessing analysis with a fit over the longitudinal distribution allows to obtain the same quantity also directly from measurements.

The first integral in the right-hand side depends only on the stationary distribution, and we call it $K_{0n,\parallel}$. If we further

suppose, as generally done to solve the Vlasov equation, that the particles execute linear synchrotron oscillations, even if it changes with the bunch population, we observe that it does not depend on time. For the second integral, which is related to the perturbation, we have

$$\begin{aligned} & \int_{-\infty}^{\infty} z^n \lambda_1(z; t) dz \\ &= \sum_{m=-\infty}^{\infty} e^{j\Delta\omega_{cn}t} \int_{-\infty}^{\infty} \int_{-\infty}^{\infty} R_{m,\parallel}(J_{\parallel}) e^{-jm\phi_{\parallel}} z^n dz d\varepsilon. \end{aligned} \quad (24)$$

The elementary area in the phase space can be written in terms of the action-angle variables, such that

$$\begin{aligned} \int_{-\infty}^{\infty} z^n \lambda_1(z; t) dz &\propto \sum_{m=-\infty}^{\infty} e^{j\Delta\omega_{cn}t} \int_0^{\infty} R_{m,\parallel}(J_{\parallel}) dJ_{\parallel} \\ &\quad \times \int_0^{2\pi} e^{-jm\phi_{\parallel}} z^n d\phi_{\parallel}. \end{aligned} \quad (25)$$

Due to the hypothesis of linear oscillations, the longitudinal position z varies sinusoidally with time and it has a dependency on the action-angle variables of the kind $z \propto \sqrt{J_{\parallel}} e^{j\phi_{\parallel}}$. From Eq. (25) we can then write

$$\begin{aligned} \int_{-\infty}^{\infty} z^n \lambda_1(z; t) dz &\propto \sum_{m=-\infty}^{\infty} e^{j\Delta\omega_{cn}t} \int_0^{\infty} R_{m,\parallel}(J_{\parallel}) J_{\parallel}^{n/2} dJ_{\parallel} \\ &\quad \times \int_0^{2\pi} e^{-j(m-n)\phi_{\parallel}} d\phi_{\parallel}. \end{aligned} \quad (26)$$

We are not interested in the proportionality constant. We further observe that the last integral is always zero except when $n = m$. In that case it is 2π , the sum over m disappears, and we remain with

$$\int_{-\infty}^{\infty} z^n \lambda_1(z; t) dz = K_{1n,\parallel} e^{j\Delta\omega_{cn}t}, \quad (27)$$

where in $K_{1n,\parallel}$ we have included all the quantities independent on time but dependent on the n th mode, such as the integral over the unknown $R_{n,\parallel}(J_{\parallel})$ function. Finally we can write

$$M_{n,\parallel} = \int_{-\infty}^{\infty} z^n \lambda(z; t) dz = K_{0n,\parallel} + K_{1n,\parallel} e^{j\Delta\omega_{cn}t}. \quad (28)$$

We are not interested in the two constants $K_{0n,\parallel}$ and $K_{1n,\parallel}$, but we observe that Eq. (28) oscillates at the frequency $\Delta\omega_{cn}$ of the coherent n th mode, and this frequency is the one that we want to determine.

In order to compare quantities having the same dimensions, we consider the n th root of the absolute value of $M_{n,\parallel}$ with its sign, which we call $S_{n,\parallel}$, of the kind

$$\begin{aligned} S_{n,\parallel} &= \pm \left| \int_{-\infty}^{\infty} z^n \lambda(z; t) dz \right|^{1/n} \\ &= \pm |K_{0n,\parallel}|^{1/n} \left| 1 + e^{j\Delta\omega_{cn}t} \frac{K_{1n,\parallel}}{K_{0n,\parallel}} \right|^{1/n} \\ &\simeq \pm |K_{0n,\parallel}|^{1/n} \left| 1 + e^{j\Delta\omega_{cn}t} \frac{K_{1n,\parallel}}{nK_{0n,\parallel}} \right|, \end{aligned} \quad (29)$$

where the sign plus or minus depends on the sign of $M_{n,\parallel}$, and we have used the assumption that the effect of the perturbation is small compared to that of the stationary distribution and have expanded the n th root to first order. We observe that $S_{n,\parallel}$ has a constant term plus a quantity that oscillates at the coherent frequency $\Delta\omega_{cn}$. If we evaluate $S_{n,\parallel}$ turn after turn for several synchrotron oscillations, and subtract its mean value $\langle S_{n,\parallel} \rangle$, we remove the constant component and remain only with the oscillating part. Therefore, the Fourier transform of this quantity is a spectrum with peaks at the frequencies of the azimuthal coherent mode n . This procedure is performed as a function of the bunch intensity so that we can obtain $\Delta\omega_{cn}$ at different values of the bunch population. Since the amplitude of the peaks depends on the mode number n , for the calculations we normalize each spectrum of $S_{n,\parallel}$ to its maximum value and then sum a given number of modes for each intensity. An example of the results by using a pure inductive impedance is shown in the left-hand side of Fig. 6, where we have represented the real part of the coherent frequency $\Delta\omega_{cn}$ of the first ten modes divided by $\Omega_0 Q_{s0}$ as a function of the bunch population. The values of $M_{n,\parallel}$ have been obtained by using the SBSC simulation code [6,7] by using 10^6 macroparticles.

At low intensity we observe coherent frequencies at multiples of the unperturbed synchrotron frequency as in the previous section. When the intensity increases, there is a moving down of these frequencies, more accentuated for higher modes. Moreover, at higher intensities, several lines start to appear for each azimuthal mode, which we interpret as produced by different radial modes of the same azimuthal family. As a comparison, in the right-hand side of the figure we show the frequency spectrum obtained by considering only the Fourier transform of $S_{2,\parallel}$, corresponding to the rms bunch length. The bunch and machine parameters are the same as those discussed in Sec. II. No instability is observed in this case up to a bunch population larger than $N_b = 2.0 \times 10^{11}$.

If the impedance has a real part, the mode coupling instability takes place. Indeed, by using the BBR impedance of Sec. II instead of a pure inductive one, from the simulations we obtain a microwave instability threshold of about $N_b = 1.2 \times 10^{11}$ particles per bunch, as we show in the next section. If we use the above described method to obtain the frequencies of the coherent modes, we have the results of the left-hand side of Fig. 7. We still observe a

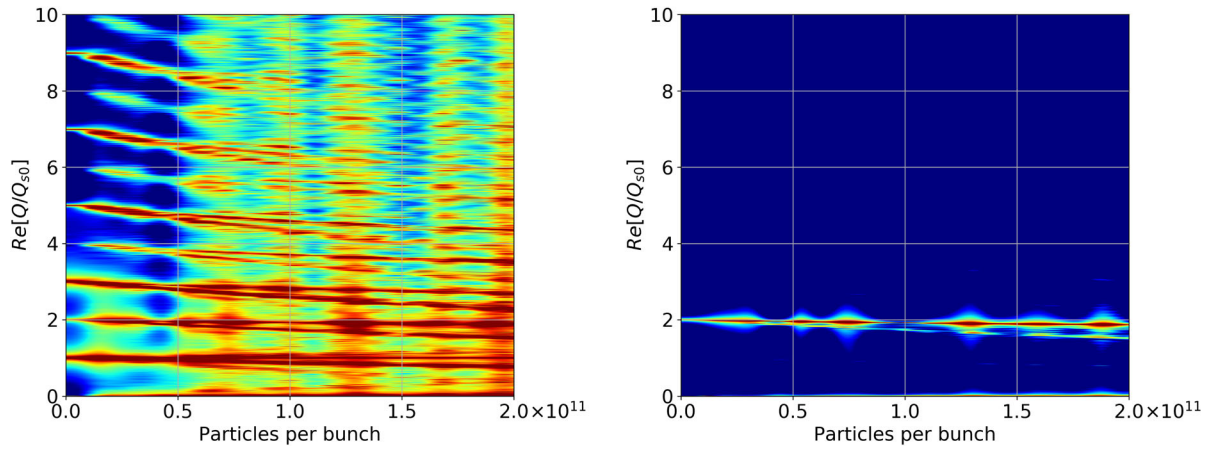


FIG. 6. Real part of normalized mode-frequency shift obtained with the results of SBSC with a pure inductive impedance above transition. The left-hand side has been obtained by summing the first ten modes, the right-hand side has been obtained by using only the rms bunch length.

coherent frequency shift of some modes with low azimuthal number, but we cannot highlight those with high number. This is due to the fact that, at the microwave threshold, for the nonlinear character of the instability, we obtain a spectrum with a very high level of noise, represented in red in the figure at intensities close to $N_b = 1.2 \times 10^{11}$. This noise hides the frequencies of coherent modes with high number.

This is better highlighted in the right-hand side of the figure, where we have represented two spectra corresponding to $N_b = 1.1 \times 10^{11}$ and $N_b = 1.2 \times 10^{11}$ particles per bunch, which is just below and above the microwave instability threshold. While at 1.1×10^{11} the lines of the different modes are well distinguishable up to about the tenth mode, as can be seen in the top plot, when the instability occurs at $N_b = 1.2 \times 10^{11}$, the background due

to the noise increases, in particular for high modes, to a level higher than the peaks of high modes of lower intensities. In this way those peaks cannot be distinguished in the 2D plot of the left-hand side.

In order to overcome this problem and to show also the coherent frequencies of these high-order modes, we can use a filter to the Fourier transform. For this purpose we have used the Hanning (or Hann) function, one of the different functions used in statistics for smoothing (see, e.g. [39]). This function is of the kind

$$w(n) = \sin^2\left(\frac{\pi n}{M}\right), \quad (30)$$

with M the total number of points for the Fourier transform. It is used in particular for smoothing discontinuities at the

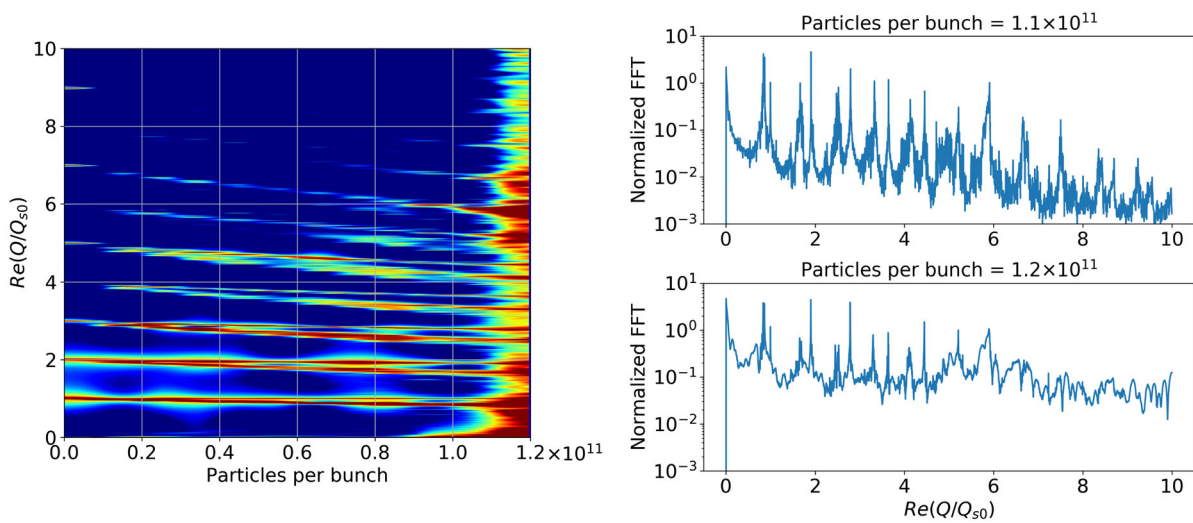


FIG. 7. Left: Real part of normalized mode-frequency shift of the first ten azimuthal coherent oscillation modes obtained with the results of SBSC with a BBR impedance. In the right-hand side two normalized spectra just below and above the microwave instability threshold are shown.

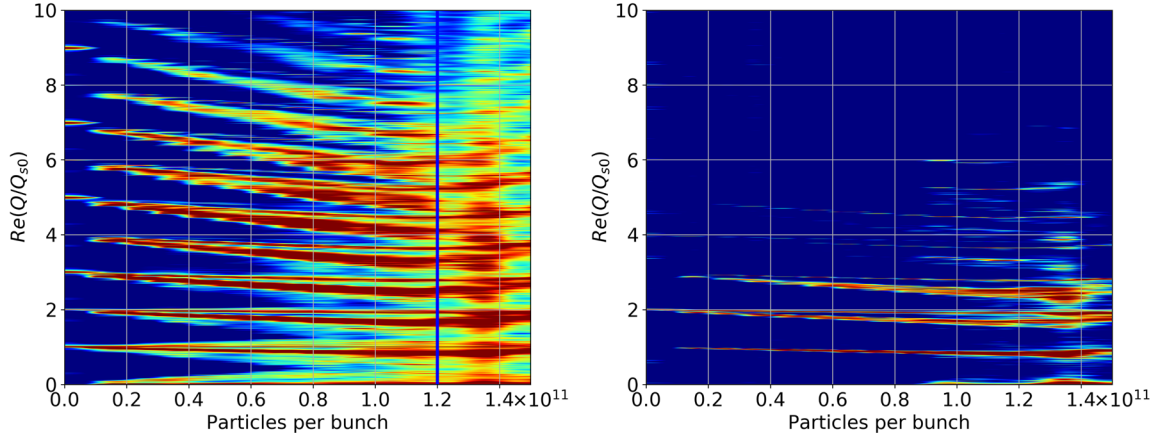


FIG. 8. Real part of normalized mode-frequency shift obtained with the results of SBSC with a BBR impedance. A Hanning window has been used for the Fourier transform. The left-hand side has been obtained by summing the first ten modes, the right-hand side has been obtained by using only the rms bunch length. The vertical blue line corresponds to the intensity threshold of the microwave instability.

beginning and end of the sampled signal. In our case, when an instability occurs, the signal is cut when oscillations have the highest amplitude and we need to taper this behavior. By multiplying the previous spectra with the Hanning window, we obtain the plot shown in the left-hand side of Fig. 8. In this way we can observe the coherent frequencies of the modes even to intensities higher than the microwave instability threshold, which corresponds to the vertical blue line in the figure. As a comparison, in the right-hand side of the same figure we show the results obtained by considering only the spectrum of $S_{2,\parallel}$, which is the rms bunch length, and we can see that only the first few modes are visible.

For the transverse plane we follow a similar procedure, but the quantity to analyze in frequency domain is different. Let us consider the 4D phase space distribution as the sum of a stationary distribution and a perturbation,

$$\Psi(z, \varepsilon, y, p_x; t) = \Psi_0(z, \varepsilon, x, p_x) + \Psi_1(z, \varepsilon, x, p_x; t), \quad (31)$$

with x and p_x the transverse position (vertical or horizontal) and its momentum. Also in this case we can expand the perturbation as a sum of coherent oscillation modes of the kind [1]

$$\Psi_1(z, \varepsilon, x, p_x; t) = e^{j\frac{\xi\omega_0 Q_{s0} z}{v\eta}} \sum_{m=-\infty}^{\infty} e^{j\Delta\omega_{cm} t} R_{m,\parallel}(J_{\parallel}) e^{-jm\phi_{\parallel}} R_{\perp}(J_{\perp}) e^{-j\phi_{\perp}}, \quad (32)$$

with v the longitudinal charge velocity. We have introduced here the transverse action-angle variables $(J_{\perp}, \phi_{\perp})$ and another unknown function $R_{\perp}(J_{\perp})$. This expansion is in analogy to Eq. (20), except for the difference that, due to the chromaticity, we now have an additional head-tail phase factor [3].

The distribution in the physical space (z, x) is

$$\begin{aligned} \rho(z, x; t) &= \int_{-\infty}^{\infty} d\varepsilon \int_{-\infty}^{\infty} dp_x \Psi(z, \varepsilon, x, p_x; t) \\ &= \int_{-\infty}^{\infty} \int_{-\infty}^{\infty} \Psi_0(z, \varepsilon, x, p_x) d\varepsilon dp_x \\ &\quad + \int_{-\infty}^{\infty} \int_{-\infty}^{\infty} \Psi_1(z, \varepsilon, x, p_x; t) d\varepsilon dp_x. \end{aligned} \quad (33)$$

Let us consider in the transverse plane the quantity

$$\begin{aligned} M_{n,\perp} &= \int_{-\infty}^{\infty} dx \int_{-\infty}^{\infty} dz x \rho(z, x; t) z^n \\ &= \int_{-\infty}^{\infty} \int_{-\infty}^{\infty} \int_{-\infty}^{\infty} \int_{-\infty}^{\infty} x \Psi_0(z, \varepsilon, x, p_x) z^n dz d\varepsilon dx dp_x \\ &\quad + \sum_{m=-\infty}^{\infty} e^{j\Delta\omega_{cm} t} \int_{-\infty}^{\infty} \int_{-\infty}^{\infty} \int_{-\infty}^{\infty} \int_{-\infty}^{\infty} R_{m,\parallel}(J_{\parallel}) \\ &\quad \times e^{j\frac{\xi\omega_0 \rho_0 z}{c\eta}} e^{-jm\phi_{\parallel}} z^n x R_{\perp}(J_{\perp}) e^{-j\phi_{\perp}} dz d\varepsilon dx dp_x. \end{aligned} \quad (34)$$

We observe here that $M_{n,\perp}$ can be obtained from simulation codes at each integration step. Moreover, if it is possible to reconstruct, turn after turn, the physical distribution in (z, x) in a real machine, the analysis can also be performed from measurements. It is also important to highlight that for $n = 0$, $M_{0,\perp}$ represents the transverse displacement of the bunch centroid.

Let us use the action-angle variables such that the elementary phase space volume is given by $d\phi_{\parallel} dJ_{\parallel} d\phi_{\perp} dJ_{\perp}$. Moreover, the hypothesis of the linear approximation for the longitudinal motion is still valid so that $z \propto \sqrt{J_{\parallel}} e^{j\phi_{\parallel}}$. The first term in the right-hand side of Eq. (34) is constant with time, and we call it $K_{0n,\perp}$, while the second one is

$$\begin{aligned}
&\propto \sum_{m=-\infty}^{\infty} e^{j\Delta\omega_{cm}t} \int_0^{\infty} R_{m,\parallel}(J_{\parallel}) J_{\parallel}^{n/2} dJ_{\parallel} \\
&\times \int_0^{2\pi} e^{j\frac{\xi\omega_{\beta 0}z}{c\eta}} e^{-j(m-n)\phi_{\parallel}} d\phi_{\parallel} \\
&\times \int_0^{\infty} \int_0^{2\pi} x R_{\perp}(J_{\perp}) e^{-j\phi_{\perp}} d\phi_{\perp} dJ_{\perp}. \quad (35)
\end{aligned}$$

The last double integral is the dipole displacement of the transverse distribution [1]. The integral in ϕ_{\parallel} is now different from that of Eq. (26) due to the presence of an additional exponential having a dependence on z . However, since z is proportional to $e^{j\phi_{\parallel}}$, then that integral reduces to

$$\int_0^{2\pi} e^{jAe^{j\phi_{\parallel}}} e^{-j(m-n)\phi_{\parallel}} d\phi_{\parallel}, \quad (36)$$

with A an arbitrary real value. This integral, as for the longitudinal case, is different from zero only if $n = m$, and in that case it is equal to 2π . Therefore, we finally obtain that

$$\begin{aligned}
M_{n,\perp} &= \int_{-\infty}^{\infty} dx \int_{-\infty}^{\infty} dz x \rho(z, x; t) z^n \\
&= K_{0n,\perp} + K_{1n,\perp} e^{j\Delta\omega_{cn}t}, \quad (37)
\end{aligned}$$

where in $K_{1n,\perp}$ we have included all the quantities independent on time but dependent on the n th mode. We observe that Eq. (37) has the same form as Eq. (28). Therefore, also in the transverse plane we can do considerations similar to the ones that we did for the longitudinal plane. In particular, the $(n+1)$ th root of $M_{n,\perp}$, which we call $S_{n,\perp}$, at the first order expansion oscillates with the coherent frequency $\Delta\omega_{cn}$. If we then evaluate $M_{n,\perp}$ turn after turn, consider its $(n+1)$ th root, subtract its mean value, perform the Fourier transform, normalize the

spectrum to its maximum value and finally sum over some modes for each intensity, we obtain spectra similar to those of the longitudinal plane but for the coherent frequencies of the transverse modes. It is worth mentioning that in this case no Hanning window has been used.

Simulations in the transverse plane to obtain $M_{n,\perp}$ have been performed with the tracking code `PyHEADTAIL` [40] and with the parameters of Sec. II. The results of the frequency analysis are shown in the left-hand side of Fig. 9. In the vertical axis ΔQ is the difference between the tunes obtained from the Fourier transform and Q_{x0} . For the plot we have summed the first ten modes. We can see a shift of the mode $n = 0$ which couples the mode $n = -1$ at an intensity of about $N_b = 3.7 \times 10^{11}$ particles per bunch. The bunch becomes stable at $N_b = 4 \times 10^{11}$ and unstable again right after. Then the coupled modes become stable at $N_b = 5.1 \times 10^{11}$ and a new instability of the modes -1 and -2 takes place at $N_b = 6 \times 10^{11}$.

If we consider only the analysis performed with the mode $n = 0$, that is $M_{0,\perp}$, which corresponds to the betatron oscillations of the centre of mass, the Fourier transform gives the results of the right-hand side of the figure. We can see that in this case it is still possible to recognize the coupling of the lower modes and the instability thresholds, however the coherent frequencies of the modes with higher index cannot be highlighted. The Fourier analysis of the betatron center of mass has been indeed used in the past to determine the transverse mode coupling threshold for the CERN SPS [34]. The study performed there gave a bit higher number of visible modes with respect to those shown in the right-hand side of Fig. 9 thanks to the use of `SUSSIX` [41], a dedicated software for the Fourier transforms. In our case, only the classical FFT algorithm was needed to obtain the left-hand side figure.

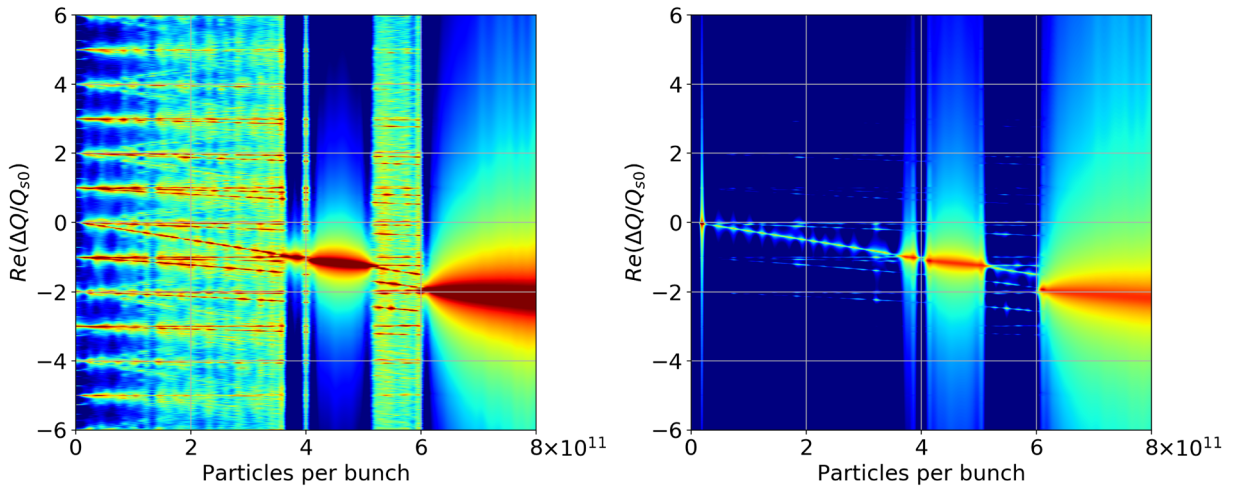


FIG. 9. Real part of normalized mode-frequency shift obtained with the results of `PyHEADTAIL` with a transverse BBR impedance. The left-hand side has been obtained by summing the first ten modes, the right-hand side has been obtained by using only $M_{0,\perp}$.

V. COMPARISONS AND RESULTS

In this section we compare the results of GALACLIC and GALACTIC with those of the simulation codes. Let us start with the longitudinal plane where two impedance models have been used, as discussed in Sec. II.

Simulations have been performed with the code SBSC, but comparisons with MuSiC [7] and BLOND [42] were performed as a cross-check. SBSC and BLOND are written in different languages (Fortran the first and C++ and PYTHON the second one), but they evaluate the wakefield effects with the same technique of slicing the bunch distribution, and they can also consider a pure inductive impedance (which has, as wakefield, a function proportional to the derivative of the Dirac delta function), while MuSiC has a totally different approach which uses a matrix formalism for the wakefield evolution fitting the generic machine impedance with the sum of resonators. In all cases, they are based on the same principles of the original work of Siemann [43]. In Fig. 10 we show the values of bunch length, the energy spread and the emittance averaged over all the simulation turns, as a function of bunch intensity obtained with the above codes for both the BBR and pure inductive impedances (for this last case MuSiC is not suited and only the other two codes were used). Error bars for the curves have been obtained performing the standard deviation of the same quantities, which are larger for unstable beams. Observe that all the curves are

superimposed up to about $N_b = 1.2 \times 10^{11}$ particles per bunch, showing a very good agreement between the codes. Above this intensity, for the case with the BBR impedance model, an anomalous increase of all the quantities takes place. This represents the threshold of the microwave instability regime. On the other hand, as we have already observed, there is no sign of instability for the pure inductive impedance case up to an intensity larger than $N_b = 2.0 \times 10^{11}$.

These results allow to better interpret Fig. 6, where we do not observe any mode coupling but only a frequency shift of the coherent oscillation modes, and Fig. 8, where a coupling of higher modes seems to occur around the microwave instability threshold. A confirmation of this behavior is given by GALACLIC, as can be seen in Figs. 11 and 12, where the results of the Vlasov solver and of the SBSC simulation code are shown for both impedances. To make the comparison easier and follow the frequency shifts of the modes given by the two codes, we have shown here again the left-hand side of Figs. 6 and 8.

We can see that the method described in Sec. IV represents very well the frequency shift of the coherent oscillation modes. In fact a very good agreement is obtained for the pure inductive impedance case, shown in Fig. 11, while a slight disagreement on the threshold can be observed for the BBR case of Fig. 12. Indeed, for a BBR, GALACLIC foresees an instability threshold a bit

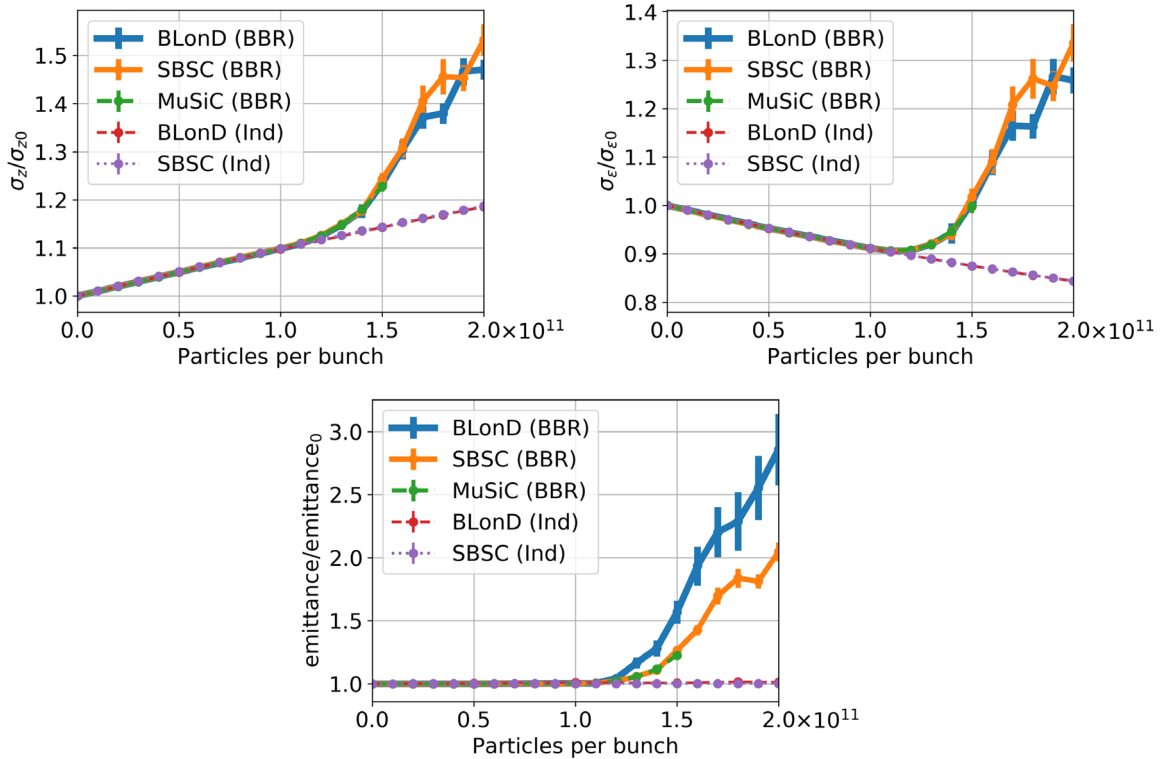


FIG. 10. Bunch length (left), energy spread (right) and emittance (bottom), normalized to their zero-intensity values, as a function of the bunch population for the BBR and pure inductive impedance obtained with different simulation codes.

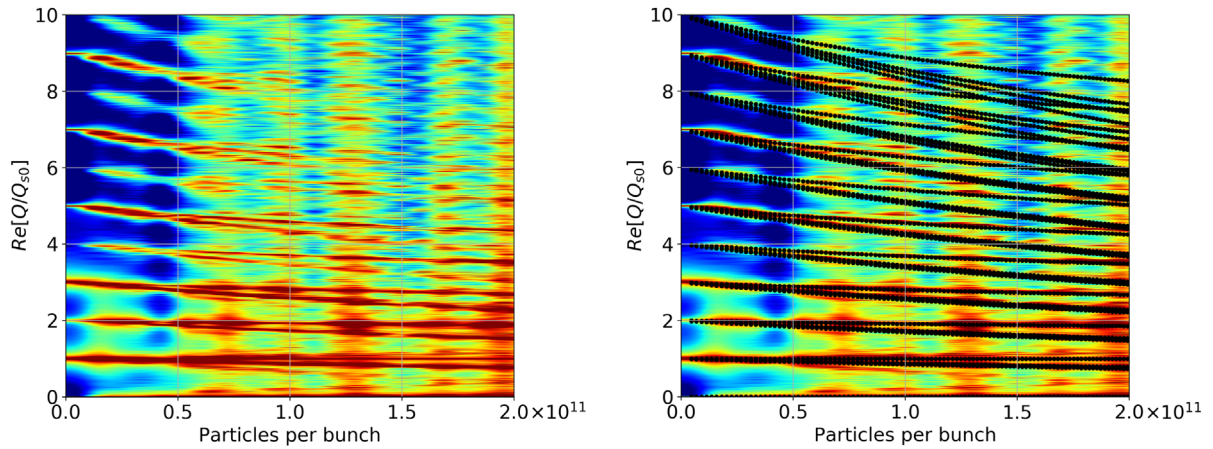


FIG. 11. Comparisons of the real part of the normalized mode-frequency shift between SBSC code and GALACLIC (black dots in the right-hand side) with the pure inductive impedance.

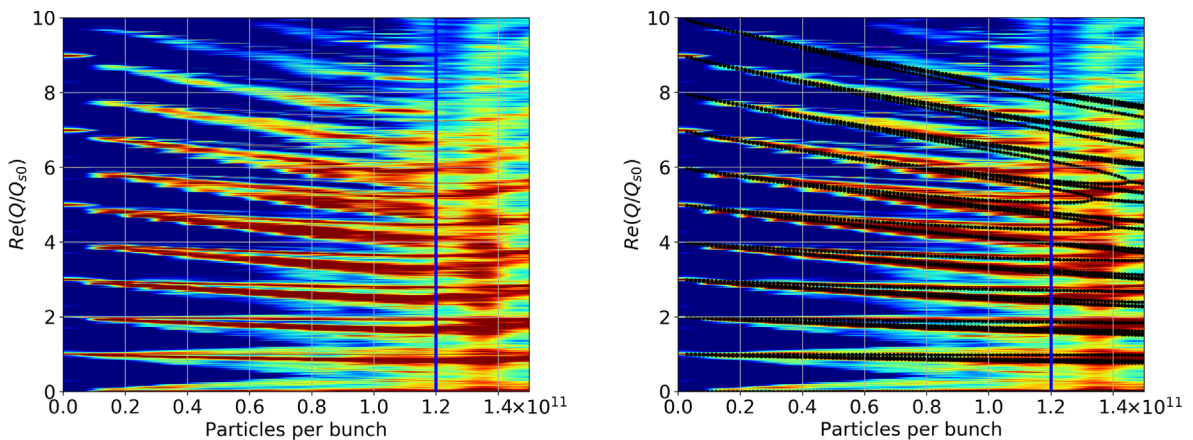


FIG. 12. Comparisons of the real part of the normalized mode-frequency shift between SBSC code and GALACLIC (black dots in the right-hand side) with the BBR impedance.

above $N_b = 1.3 \times 10^{11}$ particles per bunch, a value slightly higher than that obtained with the simulation code. We suppose that this small discrepancy at higher intensities depends on the PWD due to the real part of the impedance which, in addition to an increase of the bunch length, included in GALACLIC, also distorts a bit the bunch shape, as shown in Fig. 13. From the figure we can see that at $N_b = 1.5 \times 10^{11}$ particles per bunch there is a small asymmetry of the bunch shape with respect to the unperturbed distribution in the BBR impedance case (right-hand side of the figure) with respect to the pure inductive one. The comparison in the right-hand side of Fig. 12 shows also that the instability threshold, in this case, is determined by the coupling of higher order modes (in particular 6 and 7).

For the transverse plane [44,45], we can do a similar analysis, but we cannot use the same codes which have been developed only for the longitudinal plane. As a consequence we have used PyHEADTAIL. In this case it is

also possible to determine the instability growth rate by evaluating the exponential increase of the center of mass oscillations. An example is given in Fig. 14, where the transverse center of mass of a bunch with 6.8×10^{11} particles per bunch is shown as a function of the number of turns together with the exponential fit. Therefore, in the transverse plane, we can evaluate both the coherent frequencies of the oscillation modes and the corresponding growth rates.

The results, compared with those of GALACTIC, are shown in Figs. 15 and 16 where we can observe an excellent agreement. In Fig. 15 we have the frequencies of the coherent modes and, in Fig. 16, the growth rates of the instability as a function of the bunch intensity. Of course, with the simulation code, we can only determine the growth rates of the most unstable mode, while GALACTIC gives the growth rates of several unstable modes. This explains the multiple curves (black dots) of Fig. 16.

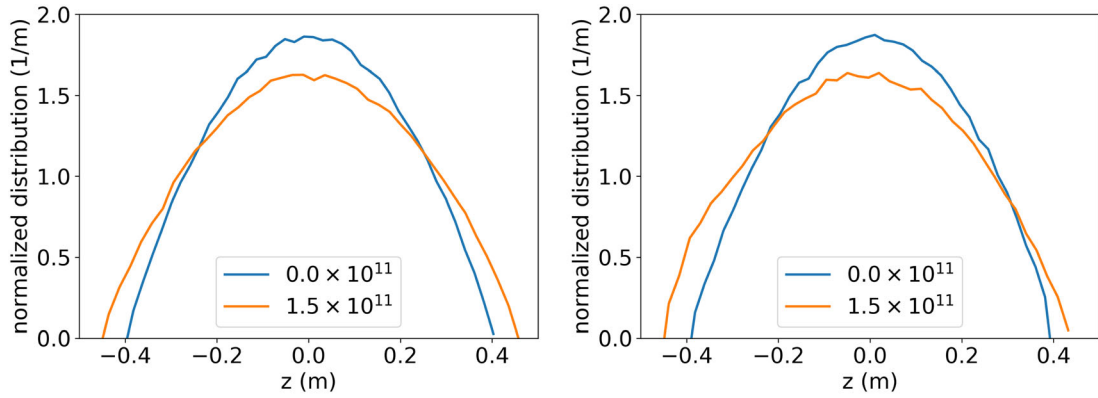


FIG. 13. Bunch shape due to the potential well distortion at zero current and at $N_b = 1.5 \times 10^{11}$ particles per bunch for the pure inductive impedance (left) and BBR (right).

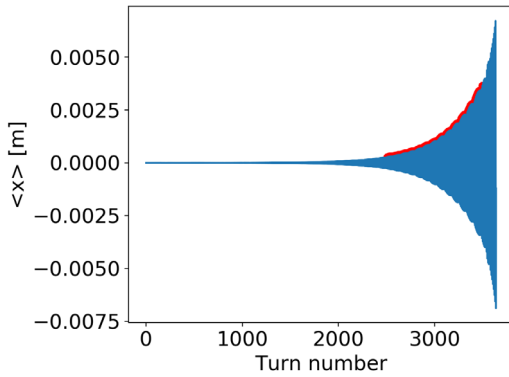


FIG. 14. Center of mass oscillations as a function of number of turns for an intensity of 6.8×10^{11} particles per bunch with the corresponding exponential fit (red curve).

VI. SIMPLE FORMULAS AND POSSIBLE MITIGATION METHODS

In the “long-bunch” regime (where $2f_r\tau_b \gg 1$), simple analytical formulas can be obtained in both longitudinal and transverse planes, which correspond to the coasting-beam formulas with peak values [29], with no dependence anymore on the synchrotron tune.

In the longitudinal plane, the stability criterion corresponds to the Keil-Schnell-Boussard criterion (i.e. the Keil-Schnell criterion for coasting beams applied with peak values for bunched beams as proposed by Boussard), whose scaling is given by [29]

$$N_{b,th}^{\parallel} \propto \frac{|\eta|\epsilon_{\parallel} \frac{\Delta p}{p_0}}{\left| \frac{Z_{\parallel}(p)}{p} \right|}, \quad (38)$$

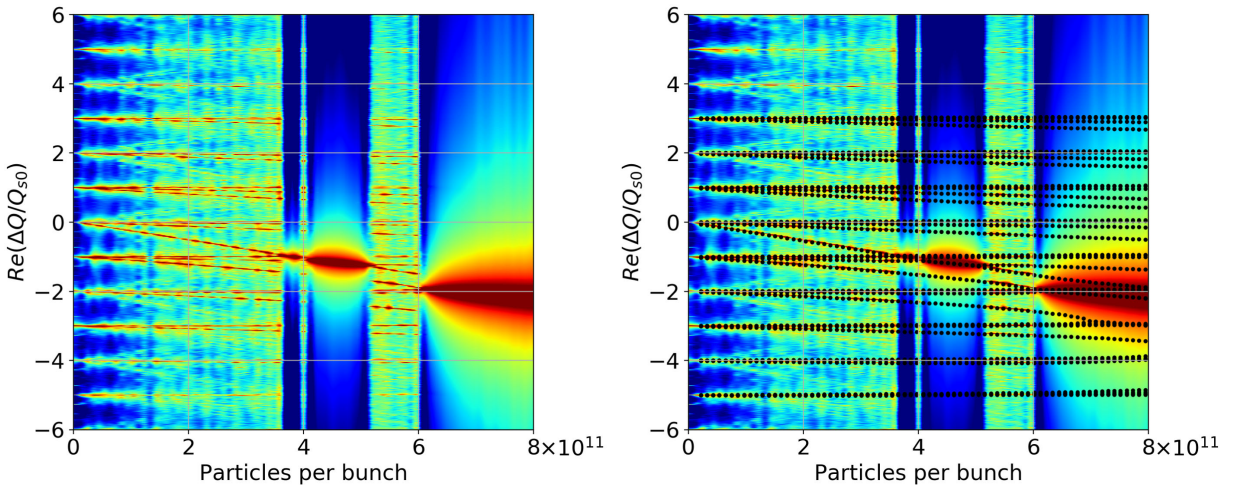


FIG. 15. Comparison of the real part of the normalized mode-frequency shift between PyHEADTAIL and GALACTIC (black dots in the right-hand side) with the transverse BBR impedance.

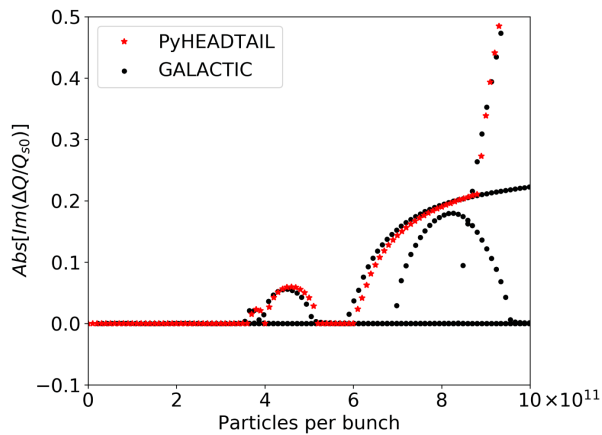


FIG. 16. Growth rates of the transverse mode coupling instability as a function of the bunch intensity given by PyHEADTAIL and GALACTIC (black dots). Observe that GALACTIC gives the growth rates of several unstable modes.

where ϵ_{\parallel} is the longitudinal emittance and $\Delta p/p_0$ the longitudinal momentum spread. Therefore, to increase the longitudinal intensity threshold one needs to reduce the impedance and/or increase the slippage factor (i.e. move further away from transition) and/or increase the longitudinal emittance and/or increase the momentum spread. Note that, as it is the product between the longitudinal emittance and the momentum spread which matters (and as protons are considered in this paper), it is more effective to increase the momentum spread than increasing the bunch length. Indeed, increasing for instance the rf voltage, and assuming that the longitudinal emittance is preserved, the momentum spread increases and therefore the longitudinal intensity threshold as well. It is worth mentioning that, as this instability is taking place between high-order modes, a bunch-by-bunch longitudinal damper is not helpful.

In the transverse plane, a similar criterion can be obtained, whose scaling is given by [46]

$$N_{b,th}^{\perp} \propto \frac{|\eta| \epsilon_{\parallel} Q_x \omega_r}{|Z_{\perp}|}. \quad (39)$$

Therefore, to increase the transverse intensity threshold, one needs to reduce the impedance (and/or increase the resonance frequency) and/or increase the slip factor (i.e. move further away from transition) and/or increase the longitudinal emittance and/or increase the transverse tune. The latter equation was successfully used in the past to significantly increase the intensity threshold at the CERN SPS (such that it is not a performance limitation anymore), even if the role of space charge still needs to be fully understood [47]. It is worth mentioning also that another mitigation method consists in increasing the chromaticity [46], as it was in fact initially done at the CERN SPS [47],

but it is usually better to try and reduce the chromaticity for beam lifetime considerations. Finally, it is also worth mentioning that a bunch-by-bunch transverse damper, which is usually present in machines operating with many bunches, can be ineffective, detrimental or beneficial for the transverse mode coupling instability depending on the parameters [33,48] (in the long-bunch regime, it is ineffective as the main instability takes place between high-order modes) and that the detuning impedance, present in axially asymmetric chambers, can also modify the intensity threshold (in the long-bunch case discussed in [49], the intensity thresholds in both transverse planes could be mainly explained by the change of the driving impedances, with a slight detrimental effect from the detuning impedance). As in the case of axially asymmetric structures, the intensity thresholds are different in the horizontal and vertical planes, linear coupling between the two transverse planes can be used to significantly raise the lowest intensity threshold [50].

VII. CONCLUSIONS

In this paper we have presented two Vlasov solvers, GALACTIC and GALACTIC, to study the single-bunch longitudinal and transverse mode coupling instability for a proton machine. We have also discussed a novel method to obtain the frequencies of the coherent oscillation modes of a bunch from the results of simulation codes. For the longitudinal plane, a good agreement has been reached between GALACTIC and SBSC for the two cases of pure inductive and BBR impedances above transition, taking into account, in the Vlasov solver, the simplest model of potential well distortion (where, for the BBR case, the shift of the synchronous phase is neglected). With a small real part of the impedance different from zero, the longitudinal microwave instability observed in Fig. 10 as an anomalous increase of bunch length, energy spread and emittance, has been explained as a longitudinal mode coupling instability (see Fig. 12 right-hand side). The intensity threshold is very close to the Keil-Schnell-Boussard criterion of Eq. (38). This equation can be also useful to determine the important parameters which can be used to increase the longitudinal intensity threshold.

An excellent agreement has also been obtained between GALACTIC and PyHEADTAIL for the case of a BBR impedance model for both the frequency shifts of the coherent modes of oscillation and the growth rates of the instability. In this case, the scaling of the intensity threshold, shown in Eq. (39), reveals how to increase the transverse intensity threshold.

Finally, the method described to obtain the frequencies of the coherent modes of oscillation from the results of longitudinal and transverse simulation codes can also be applied to data measurements if the bunch distribution in the physical space can be reconstructed turn by turn.

ACKNOWLEDGMENTS

This work was partially supported by the European Commission under the HORIZON2020 Integrating Activity project ARIES, Grant Agreement No. 730871, and by INFN National committee V through the ARYA project.

-
- [1] A. W. Chao, *Physics of Collective Beam Instabilities in High Energy Accelerators* (John Wiley & Sons, New York, 1993).
- [2] L. Palumbo, V. G. Vaccaro, and M. Zobov, Wakefields and impedance, CERN Technical Report No. 95-06, CERN, Geneva, Switzerland, 1995, [arXiv:physics/0309023](https://arxiv.org/abs/physics/0309023).
- [3] K. Y. Ng, *Physics of Intensity Dependent Beam Instabilities* (World Scientific, Singapore, 2006).
- [4] E. Belli, P. C. Pinto, G. Rumolo, A. Sapountzis, T Sinkovits, M. Taborelli, B. Spataro, M. Zobov, G. Castorina, and M. Migliorati, Electron cloud buildup and impedance effects on beam dynamics in the future circular $e^+ e^-$ collider and experimental characterization of thin TiZrV vacuum chamber coatings, *Phys. Rev. Accel. Beams* **21**, 111002 (2018).
- [5] S. Persichelli, M. Migliorati, N. Biancacci, S. Gilardoni, E. Métral, and B. Salvant, Transverse beam coupling impedance of the CERN Proton Synchrotron, *Phys. Rev. Accel. Beams* **19**, 041001 (2016).
- [6] M. Migliorati, S. Persichelli, H. Damerau, S. Gilardoni, S. Hancock, and L. Palumbo, Beam-wall interaction in the CERN Proton Synchrotron for the LHC upgrade, *Phys. Rev. ST Accel. Beams* **16**, 031001 (2013).
- [7] M. Migliorati and L. Palumbo, Multibunch and multi-particle simulation code with an alternative approach to wakefield effects, *Phys. Rev. ST Accel. Beams* **18**, 031001 (2015).
- [8] M. Migliorati, S. Aumon, E. Koukovini-Platia, A. Huschauer, E. Métral, G. Sterbini, and N. Wang, Instability studies at the CERN proton synchrotron during transition crossing, *Phys. Rev. Accel. Beams* **21**, 120101 (2018).
- [9] M. Borland, ELEGANT: A flexible SDDS-compliant code for accelerator simulation, in the *6th International Computational Accelerator Physics Conference (ICAP 2000)*, Darmstadt, Germany (2000), <https://doi.org/10.2172/761286>.
- [10] G. Bassi, A. Blednykh, and V. Smaluk, Self-consistent simulations and analysis of the coupled-bunch instability for arbitrary multibunch configurations, *Phys. Rev. Accel. Beams* **19**, 024401 (2016).
- [11] M. Migliorati, L. Palumbo, C. Zannini, N. Biancacci, and V. G. Vaccaro, Resistive wall impedance in elliptical multilayer vacuum chambers, *Phys. Rev. Accel. Beams* **22**, 121001 (2019).
- [12] M. Migliorati, E. Belli, and M. Zobov, Impact of the resistive wall impedance on beam dynamics in the future circular $e^+ e^-$ collider, *Phys. Rev. Accel. Beams* **21**, 041001 (2018).
- [13] K. L. F. Bane and G. Stupakov, Resistive wall wakefield in the LCLS undulator, in *Proceedings of the 21st Particle Accelerator Conference, Knoxville, TN, 2005* (IEEE, Piscataway, NJ, 2005), p. 3390.
- [14] K. Yokoya, Resistive wall impedance of beam pipes of general cross section, Part. Accel. **41**, 221 (1993); <https://inspirehep.net/literature/353231>.
- [15] M. Migliorati, N. Biancacci, M. R. Masullo, L. Palumbo, and V. G. Vaccaro, Space charge impedance and electromagnetic fields in elliptical vacuum chambers, *Phys. Rev. Accel. Beams* **21**, 124201 (2018).
- [16] S. Persichelli, N. Biancacci, M. Migliorati, L. Palumbo, and V. G. Vaccaro, Electromagnetic fields and Green's functions in elliptical vacuum chambers, *Phys. Rev. Accel. Beams* **20**, 101004 (2017).
- [17] U. Niedermayer, O. Boine-Frankenheim, and H. De Gerssem, Space charge and resistive wall impedance computation in the frequency domain using the finite element method, *Phys. Rev. ST Accel. Beams* **18**, 032001 (2015).
- [18] L. Wang and Y. Li, Analysis of the longitudinal space charge impedance of a round uniform beam inside parallel plates and rectangular chambers, *Phys. Rev. ST Accel. Beams* **18**, 024201 (2015).
- [19] N. Biancacci, F. Caspers, J. Kuczerowski, E. Métral, N. Mounet, B. Salvant, A. Mostacci, O. Frasciello, and M. Zobov, Impedance simulations and measurements on the LHC collimators with embedded beam position monitors, *Phys. Rev. Accel. Beams* **20**, 011003 (2017).
- [20] G. V. Stupakov, High-frequency impedance of small-angle collimators, SLAC Technical Report No. SLAC-PUB-9375, SLAC, Stanford, CA, 2002.
- [21] B. Salvant *et al.*, Building the impedance model of a real machine, in *Proceedings of the 10th International Particle Accelerator Conference (IPAC'19), Melbourne, Australia, 2019*, No. 10 in International Particle Accelerator Conference (Geneva, Switzerland, 2019), pp. 2249–2254, <https://doi.org/10.18429/JACoW-IPAC2019-WEYPLS1>.
- [22] A. Hofmann and J. R. Maidment, Current dependent phenomena in LEP, CERN Technical Report No. CERN-LEP-NOTE-168, 1979.
- [23] A. Hofmann and B. Zotter, Improved impedance models for high-energy accelerators and storage rings, CERN Technical Report No. CERN-LEP/TH-88-51, 1988.
- [24] S. Heifets, Broadband impedance of the B factory, SLAC Technical Report No. SLAC-PUB-6123, Stanford, CA, 1993.
- [25] K. L. Bane, The calculated longitudinal impedance of the SLC damping rings, in *Proceedings of the 1st EPAC Conference, Rome, Italy, 1988*, edited by S. Tazzari (1988), Vol. 1, p. 2.
- [26] Y. H. Chin, Users guide for new MOSES version 2.0: Mode-coupling single bunch instability in an electron storage ring, CERN Technical Report No. CERN/LEP-TH/88-05, Geneva, Switzerland, 1988.
- [27] A. Burov, Nested head-tail Vlasov solver, *Phys. Rev. ST Accel. Beams* **17**, 021007 (2014).
- [28] N. Mounet, Vlasov solvers and macroparticle simulations, in *Proceedings of the ICFA Mini-Workshop on Impedances and Beam Instabilities, Benevento, Italy, 2017*, edited by V. Brancolini, G. Rumolo, M. R. Masullo, and S. Petracca (CERN, Geneva, 2018), p. 77, <https://doi.org/10.23732/CYRCP-2018-001>.
- [29] J. L. Laclare, Bunched beam coherent instabilities, CERN Technical Report No. CERN-1987-003-V-1, 1987.

- [30] E. Métral, GALACTIC and GALACLIC: Two Vlasov solvers for the transverse and longitudinal planes, in *Proceedings of the 10th International Particle Accelerator Conference (IPAC19), Melbourne, Australia*, edited by M. Boland, H. Tanaka, D. Button, R. Dowd, V. R. W. Schaa, and E. Tan (2019), p. 312, <https://doi.org/10.18429/JACoW-IPAC2019-MOPGW087>.
- [31] J. P. Garnier, *Instabilités cohérentes dans les accélérateurs circulaires*, Ph.D. thesis, Institut National Polytechnique de Grenoble, Grenoble, France, 1987.
- [32] E. Métral, Intrabunch motion, CERN Technical Report No. CERN-ACC-NOTE-2020-0018, Geneva, Switzerland, 2020.
- [33] E. Métral, D. Amorim, S. Antipov, N. Biancacci, X. Buffat, and K. Li, Destabilizing effect of the LHC transverse damper, in *the 9th International Particle Accelerator Conference (IPAC18), Vancouver, Canada*, S. Koscielniak, T. Satogata, V. R. W. Schaa, and J. Thomson (2018), p. 3076, <https://doi.org/10.18429/JACoW-IPAC2018-THPAF048>.
- [34] B. Salvant, Impedance model of the CERN SPS and aspects of LHC single-bunch stability, Ph.D. thesis, École Polytechnique Fédérale de Lausanne, Lausanne, CH, 2010.
- [35] Y. Cai, Linear theory of microwave instability in electron storage rings, *Phys. Rev. ST Accel. Beams* **14**, 061002 (2011).
- [36] P. Schönfeldt, M. Brosi, M. Schwarz, J. L. Steinmann, and A.-S. Müller, Parallelized Vlasov-Fokker-Planck solver for desktop personal computers, *Phys. Rev. Accel. Beams* **20**, 030704 (2017).
- [37] R. L. Warnock, Study of bunch instabilities by the non-linear Vlasov Fokker Planck equation, *Nucl. Instrum. Methods Phys. Res., Sect. A* **561**, 186 (2006).
- [38] S. Hancock, P. Knaus, and M. Lindroos, Tomographic measurements of longitudinal phase space density, in *Proceedings of the 6th European Particle Accelerator Conference, Stockholm, 1998* (IOP, London, 1998), pp. 1520–1522.
- [39] O. M. Essenwanger, *Elements of Statistical Analysis* (Elsevier/Academic Press, Amsterdam, 1986).
- [40] PyHEADTAIL, <https://github.com/PyCOMPLETE/PyHEADTAIL>.
- [41] R. Bartolini and F. Schmidt, Computer code for frequency analysis of nonlinear betatron motion, CERN Technical Report No. CERN SL-Note-98-017-AP, Geneva, Switzerland, 1998.
- [42] BLOND, <https://blond.web.cern.ch>.
- [43] R. H. Siemann, Computer models of instabilities in electron storage rings, Cornell Technical Report No. CLNS 84/626, Cornell University, Ithaca, NY, 1984.
- [44] J. Gareyte, Transverse mode coupling instabilities, *AIP Conf. Proc.* **592**, 260 (2001).
- [45] R. D. Kohaupt, Transverse instabilities in petra, in *the 11th International Conference on High-Energy Accelerators: Geneva, Switzerland, 1980, Basel*, edited by W. S. Newman, (1980), pp. 562–565.
- [46] E. Métral, Stability criteria for high-intensity single-bunch beams in synchrotrons, in *Proceedings of the 8th European Particle Accelerator Conference, Paris, 2002* (EPS-IGA and CERN, Geneva, 2002), p. 1532.
- [47] E. Métral *et al.*, Space charge and transverse instabilities at the CERN SPS and LHC, in *the 13th International Computational Accelerator Physics Conference (ICAP2018), Key West, Florida*, edited by V. R. W. Schaa, K. Makino, P. Snopok, and M. Berz (2018), p. 80, <https://doi.org/10.18429/JACoW-ICAP2018-SUPAG01>.
- [48] E. Métral, Landau damping for TMCI: with vs without transverse damper, CERN Technical Report No. CERN-ACC-NOTE-2019-0018, Geneva, Switzerland, 2019.
- [49] E. Métral, X. Buffat, and G. Rumolo, Transverse mode-coupling instability in the presence of detuning impedance, CERN Technical Report No. CERN-ACC-NOTE-2020-0019, Geneva, Switzerland, 2020.
- [50] E. Métral and G. Rumolo, Simulation study on the beneficial effect of linear coupling for the transverse mode-coupling instability in the CERN super proton synchrotron, in *Proceedings of the 10th European Particle Accelerator Conference, Edinburgh, Scotland, 2006* (EPS-AG, Edinburgh, Scotland, 2006), p. 2916.